Journal of Alloys and Compounds 846 (2020) 156486

Contents lists available at ScienceDirect

Journal of Alloys and Compounds

journal homepage: http://www.elsevier.com/locate/jalcom

The Fe–Ga phase diagram: Revisited

A.K. Mohamed [a, **], V.V. Palacheva [a], V.V. Cheverikin [a], E.N. Zanaeva [a], W.C. Cheng [b], V. Kulitckii [c], S. Divinski [c], G. Wilde [c], I.S. Golovin [a, *]

[a] National University of Science and Technology "MISIS", Leninsky Ave. 4, 119049, Moscow, Russia
[b] National Taiwan University of Science and Technology, Taipei, 106, Taiwan, ROC
[c] University of Munster, Wilhelm-Klemm-Str. 10, 48149, Münster, Germany

ARTICLE INFO

Article history:
Received 23 May 2020
Received in revised form
19 July 2020
Accepted 20 July 2020
Available online 24 July 2020

Keywords:
Fe–Ga phase diagram
Magnetostrictive materials
XRD
TEM
VSM
SEM-EBSD study

ABSTRACT

The microstructures and phase compositions of Fe–Ga alloys with Ga contents from 15 to 45 at.% are investigated in detail applying prolonged annealing treatments at temperatures below 600 °C. X-ray diffraction (XRD), transmission electron microscopy (TEM), vibrating-sample magnetometry (VSM), and Electron backscatter diffraction (EBSD) coupled with scanning electron microscopy (SEM) methods were used in this investigation. The results are compared with predictions of four existing Fe–Ga phase diagrams proposed by W. Köster et al. (1977), J. Bras et al. (1977), O. Kubaschewski (1982), and H. Okamoto (1993). Several important inconsistencies are found and required corrections of the positions of three equilibrium boundaries. Below 400 °C, an incomplete, if any, transition from a metastable (A2 or $D0_3$) to the equilibrium ($L1_2$) state is seen after annealing for 300 h. Alloys with 25.5–28.1%Ga annealed at 450–500 °C for 300 h exhibit only the equilibrium $L1_2$ phase. Annealing at 575 °C for 300 h leads to an incomplete transition, too, indicating that the highest transition rate occurs at 100–150 °C undercooling.

1. Introduction

The structure and phase composition of Fe–Ga alloys have been investigated through the last decades [1–13] with diverse techniques including X-ray diffraction, light microscopy, calorimetry, dilatometry, and Mössbauer spectroscopy. Most recently, special attention has been paid to the ordering of the bcc-derivative phases. The main features of the Fe–Ga phase diagram were deduced by identifying the liquidus and solidus curves [1]. The range for the Fe_6Ga_5 phase in the phase diagram has been identified by Köster et al. [2,3], which was not considered in Ref. [1]. The β-Fe_6Ga_5 phase forms via a peritectoid reaction B2 + Fe_3Ga_4 ↔ β-Fe_6Ga_5 at 800 °C, and it transforms polymorphically to α-Fe_6Ga_5 below 778 °C.

The $L1_2$ phase is found to be stable up to a temperature of 600 °C with a composition varying from 29 to 33%Ga (in this paper we use only atomic percentage), according to Ref. [1,7]. Köster et al. identified two different types of the Fe_3Ga compound. First, the α-Fe_3Ga ($L1_2$) is stable until 605 and 619 °C with a composition range between 26.1 and 29.5% Ga, respectively. Secondly, the β-Fe_3Ga ($D0_{19}$) phase is stable above these temperatures up to 681 °C for 27.5% Ga where it transforms to the α″ (B2′) phase. The concentration of 47.5%Ga corresponds to the maximum Ga solubility in bcc iron (A2). Freezing of the B2 phase inside the structure by quenching from its high temperature range was used in Ref. [4,7]. The equilibrium phase $D0_3$ was identified by Köster et al. in the concentration range of 21–26% Ga for the temperature range of 580–680 °C [2,3].

At the same time as Köster, J. Bras et al. (1977) published a different diagram with wider $L1_2$ and $D0_{19}$ regions and narrower $D0_3$ region [9]. The Fe–Ga phase diagram by O. Kubaschewski [11] is based on the data by Köster et al. [3], and it has become the most widely used Fe–Ga phase diagram. In the Fe–Ga phase diagram by Okamoto [8], several boundaries are shifted in the opposite direction compared with [9]. For example, and not exclusively, the $L1_2$ single-phase region is reduced to the range from 26.8 to 28.6%Ga. This phase diagram also proposes the narrowest range for the equilibrium A2 phase at low (below 450 °C) temperatures. O. Ikeda et al. used conventional diffusion couple technique and microstructural investigations to determine ranges for A2, B2, $D0_3$, $L1_2$, and $D0_{19}$ phases in the Fe-rich part of the Fe–Ga binary system [13]. They found that all the boundaries below 25%Ga almost coincide with the Okamoto phase diagram [8] and suggested a wider single

* Corresponding author. Leninsky Ave 4, 119049, Moscow, Russia.
** Corresponding author.
E-mail addresses: abdelkarim.abdelkarim@feng.bu.edu.eg (A.K. Mohamed), i.golovin@misis.ru (I.S. Golovin).

https://doi.org/10.1016/j.jallcom.2020.156486
0925-8388/

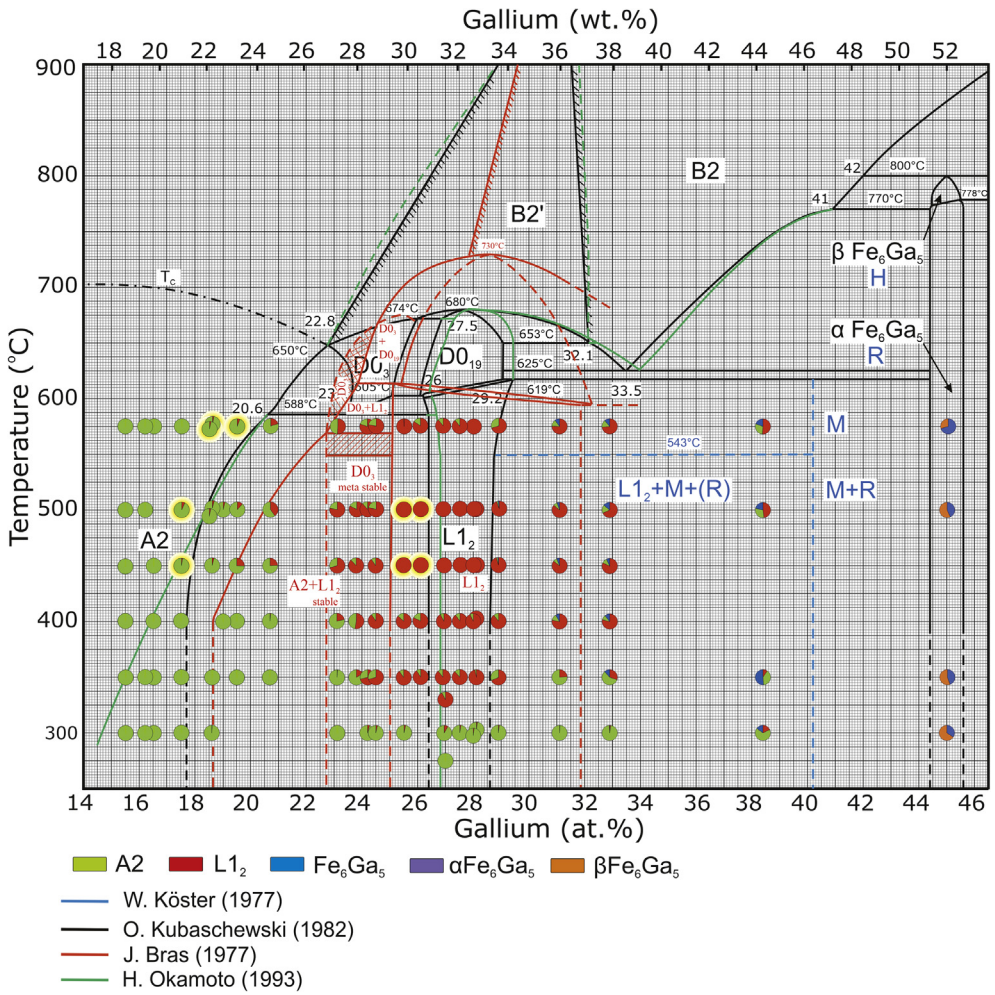

Fig. 1. Multi layered Fe–Ga equilibrium phase diagrams adapted from Refs. [3,8,9,11] and plotted together. The alloys structures after 300 h annealing are represented by pie-type charts (circles). Green, red, and blue colors represent the A2 (or DO_3), $L1_2$, Fe_6Ga_5 structures, correspondingly. For the Fe–45%Ga composition, dark blue and orange colors represent the α- and β-Fe_6Ga_5 phases, respectively. The yellow-encircled symbols indicate the alloys which phase compositions disagree with the predictions of the phase diagram after Kubaschewski [11]. (For interpretation of the references to color in this figure legend, the reader is referred to the Web version of this article.)

$L1_2$ phase region that reaches to about 30%Ga and 690 °C. Finally, a phase diagram was recently calculated using the CALPHAD-type Thermocalc database [10].

In addition to the equilibrium phases, W. Köster et al. outlined the effect of heating and cooling rates on the Fe–Ga phase transitions from metastable to stable states in their phase diagram [2,3,12]. Another metastable phase diagram was proposed by O. Ikeda et al. as a result of the growing interest in Fe–Ga alloys in the 21st millennium [13].

The aim of this study is to analyze the transition rates from metastable (as-cast) to equilibrium states and to check the existing phase diagrams in the temperature range below 600 °C, i.e., in the range where the metastable phases in as-cast alloys transform to their equilibrium states. Earlier we studied this transition in the *ex-* and *in-situ* regimes [14–18] which indicated several crucial inconsistencies and contradictions between the different versions of the reported phase diagrams but, as a rule of thumb, those annealing times were relatively short (up to 10 h) except only for a composition of Fe–27%Ga [17]. This appealed strongly for a systematic examination of the phase evolution on prolonged time scales.

2. Materials and methods

Induction melting was used to melt Fe (of commercial purity) and Ga (99.99%) followed by casting and rapid solidification in a copper mold to produce twenty four Fe–xGa alloys with x = 15–45% under protective high-purity argon gas using an Indutherm MC-20 V mini furnace. The chemical composition of the produced ingots was checked by Energy Dispersive X-ray Spectroscopy (EDX). The EDX tolerance is ±0.1% after careful calibration by measuring standard samples with a purity of 99.9999% of each element. The standard error of measurements of the chemical composition is 0.1–0.2%.

The structure of the long-term annealed samples was crystallographically analyzed by using a Bruker D8 Advanced diffractometer with Cu K_α radiation at room temperature XRD. The samples were wrapped in tantalum foil and placed in quartz ampules. Annealing treatments were carried out in argon atmosphere (99.999% purity) during 300 h at different set temperatures: 300, 350, 400, 450, 500, and 575 °C. The temperatures were measured with an accuracy of 1 °C. After annealing, the ampoules were cooled with calm air.

Scanning electron microscopy (SEM) operating at 20 kV using a TESCAN VEGA LMH microscope with a LaB_6 cathode and an energy

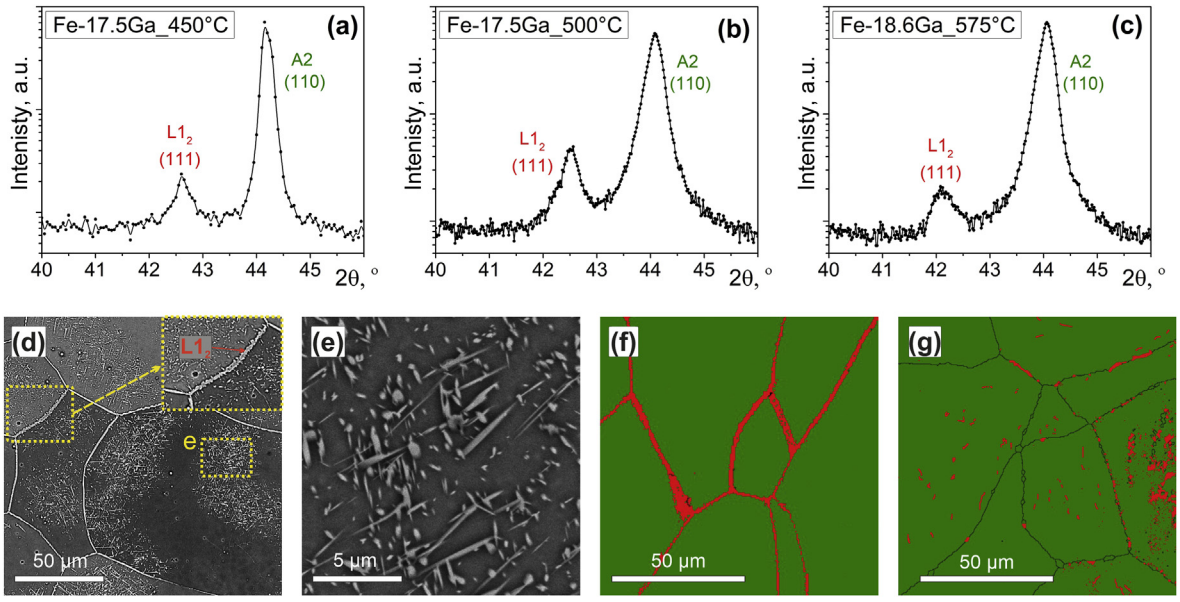

Fig. 2. XRD patterns for the Fe−17.5%Ga alloy annealed at 450 (a), 500 °C (b) and Fe−18.6%Ga annealed at 575 °C (c) for 300 h. Note that the intensity is graphically re-scaled in logarithmic scale. The SEM images for the Fe−17.5%Ga alloy annealed at 500 °C (d), with higher magnification for the area "e" showing needle-shaped $L1_2$ precipitates in the grains (e), and the EBSD image for the same sample of selected area with a large amount of $L1_2$ phase (red color) at grain boundary (f) and in grain body (g). (For interpretation of the references to color in this figure legend, the reader is referred to the Web version of this article.)

dispersive X-ray microanalysis system (Oxford Instruments, Software Advanced AZtecEnergy) was used to analyze the microstructures of the samples. Additionally, the structure of selected alloys was examined by transmission electron microscopy (TEM) using a FEI Tecnai G2 F-20 microscope operated at 200 kV.

Magnetization (VSM) curves were obtained using a VSM-130 vibrating sample magnetometer with a heating rate of 6 °C/min under a magnetic field of ≈800 kA/m.

3. Results and discussion

All as cast Fe−Ga alloys studied here presented metastable structures at room temperature, in fact either A2, $D0_3$, B2 or β-Fe_6Ga_5. The structures of as-cast Fe−(9−33%)Ga alloys were recently reported in our papers [19−21] and for as-cast Fe−38.4 and 45% Ga alloys this data will be published elsewhere. The Fe−(15−45%)Ga alloys can be divided into five groups according to their metastable structures as follows:

1. Ga < 20%, A2 structure,
2. 20% < Ga < 27%, $D0_3$ clusters embedded into an A2 matrix (there is a possibility for the existence of a small amount of B2 inclusions),
3. 27% < Ga < 31%, $D0_3$ and B2 structures,
4. 31% < Ga < 38%, B2 or $D0_3$+Fe_6Ga_5 phase,
5. Ga = 45%, the Fe_6Ga_5 phase (this phase has two polymorphic modifications, namely high and low temperature ones denoted as β (or H) and α (or R), respectively. The α/β designation was used by Kubaschewski [11] and the H/R one was used by Köster et al. [3,12]).

Long-term annealing was carried out to reach the equilibrium state. Below 300 °C no phase transition from the metastable state of the as cast alloys to the equilibrium state was observed (Fig. 1). Most of the XRD tests were done using bulk samples. About one quarter of all the tested bulk samples, including those with structures that were different compared to the equilibrium structures proposed by the existing phase diagrams, were also used to prepare powders. Additional XRD tests were carried out using these powders to confirm the results on the bulk samples. Two different methods were used to estimate the phase fractions for the studied samples:

1) the heights of the 110_{A2} (=220_{D0_3}) and 111_{L1_2} peaks are compared (Fig. 2),
2) the areas under all the peaks corresponding to each phase are compared.

The difference between these two methods does not exceed 2%. The ratios for the phase fractions are represented in Fig. 1 by the pie-type charts on top of the multi layered Fe−Ga phase diagrams [3,8,9,11]. Green color stands for the bcc and bcc-derived $D0_3$ phase, and red color represents the equilibrium fcc-derived $L1_2$ phase.

Alloys with 25.5−28.1%Ga reveal the equilibrium $L1_2$ state after annealing at 450 and 500 °C for 300 h. Below and above these temperatures, the transition is not complete, i.e., 300 h annealing is not sufficient to yield 100% of the equilibrium $L1_2$ structure in these alloys, even annealing for 720 h is insufficient to obtain the equilibrium state as reported in Ref. [22]. This behavior corroborates the Time-Temperature-Transformation (TTT) diagram [17], which explains the nose-type temperature dependence of the transition rates for the alloys with about 27%Ga. All the Fe−(17.5−45)%Ga alloys follow a similar behavior during the transition from metastable to equilibrium states during long-term annealing. Alloys with Fe−(31−45%)Ga exhibit a three-phase structure, i.e., a mixture of $D0_3$ (or B2), $L1_2$, and α- or β-Fe_6Ga_5 phases after long-term annealing.

The alloy Fe−17.5%Ga was found to show some amounts of the equilibrium phase $L1_2$ after annealing at 450 and 500 °C for 300 h (Fig. 2a and b). This fact substantiates the necessity to shift the A2/(A2 + $L1_2$) boundary to a lower Ga content. It is further supported by the experimental results for Fe−18.5, 18.6 and 19.5%Ga alloys annealed at 575 °C, which still exhibit 2−6% of $L1_2$ phase (Fig. 2c). The XRD results are confirmed by the SEM-EBSD images for the

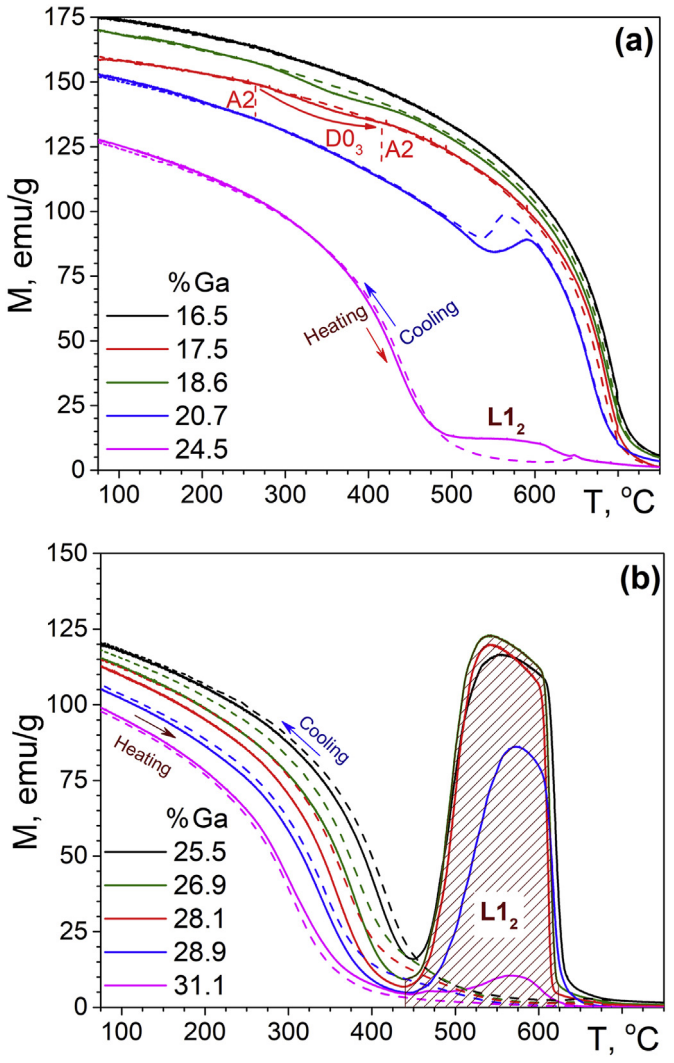

Fig. 3. Magnetization dependences on temperature during heating and cooling (dotted lines) for Fe–Ga alloys with Ga = 16.5, 17.5, 18.6, 20.7, 24.5% (a) and Ga = 25.5, 26.9, 28.1, 28.9, 31.1% (b).

Fe–17.5Ga alloy annealed at 500 °C for 300 h shown in Fig. 2d–g. It is obvious that the $L1_2$ phase originated at grain boundaries (Fig. 2d and f) and in the grains with needle-shaped precipitates (Fig. 2e and g). Fig. 2e is a high magnification image for area "e" in Fig. 2d. The EDX analysis exhibits that the needle-shaped $L1_2$ precipitates have an average Ga content of 18.7%, while the A2/$D0_3$ matrix has a concentration of 17.5%Ga.

Regarding the position of the (A2 + $L1_2$)/$L1_2$ phase boundary of the phase diagram, our experiments confirm the phase diagram by J. Bras et al. [9]. Furthermore, all the annealed samples of the Fe–28.9%Ga alloy do not demonstrate a single $L1_2$ structure at all, which is in a good agreement with the Fe–Ga phase diagrams by Köster et al. and by Kubaschewski [3,11].

By introducing the recommended changes, namely, by shifting the boundary delimiting the A2 phase and A2+$L1_2$ phase mixture regions on the phase diagram towards lower Ga concentrations, the lever rule would reproduce well all our results for the Fe–(17.5–24.5)%Ga long-term annealed samples. This is especially true for the samples annealed at 450 and 500 °C, i.e., at the temperature at which the metastable to equilibrium transition is completed by annealing for 300 h.

VSM tests were carried out to investigate the transition from metastable to equilibrium states. The magnetization for the first group of the alloys with the metastable A2 structure is higher than that of the second group with $D0_3$ + A2. The presence of a volume fraction of the B2 phase instead of the A2 phase in the third group of alloys further decreases the magnetization. The observed stronger decrease in the fourth and fifth groups results from the presence of the non-magnetic Fe_6Ga_5 phase in addition to the $D0_3$ or B2 phases in the fourth group or the absence of any magnetic phase in the fifth group (Fig. 3). By heating, the magnetization decreases featuring several effects due to the transition between the phases with different magnetization:

- Fe–(15.5–18.6)%Ga shows a uniform decrease of the magnetization which diminishes at the Curie temperature,
- Fe–(25.5–28.1)%Ga shows first a decreasing magnetization (for $D0_3$) that is reversed due to the growth of the ferromagnetic $L1_2$ phase (at 400–450 °C).

Continuous heating of Fe–17.5%Ga induces a specific response of

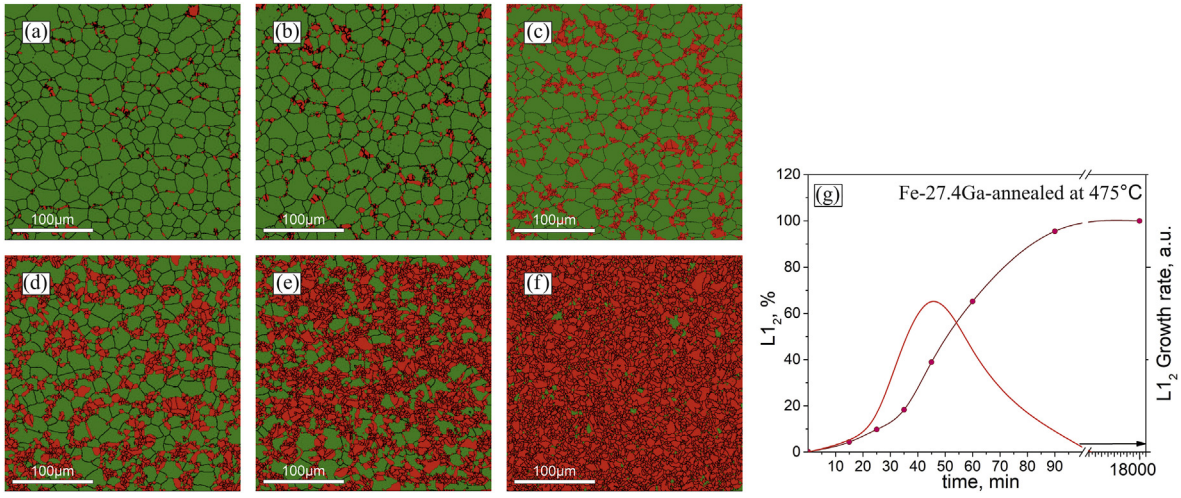

Fig. 4. SEM-EBSD structures of Fe–27.4%Ga alloy after annealing at 475 °C for 15 (a), 25 (b), 35 (c), 45 (d), 60 (e) and 90 min (f), green color represents the bcc-originated (A2, $D0_3$) phases and red color represents the $L1_2$ phase. These colors are also used in Fig. 1 to indicate the phase ratios. (g) The dependence of the %$L1_2$ on the annealing time. (For interpretation of the references to color in this figure legend, the reader is referred to the Web version of this article.)

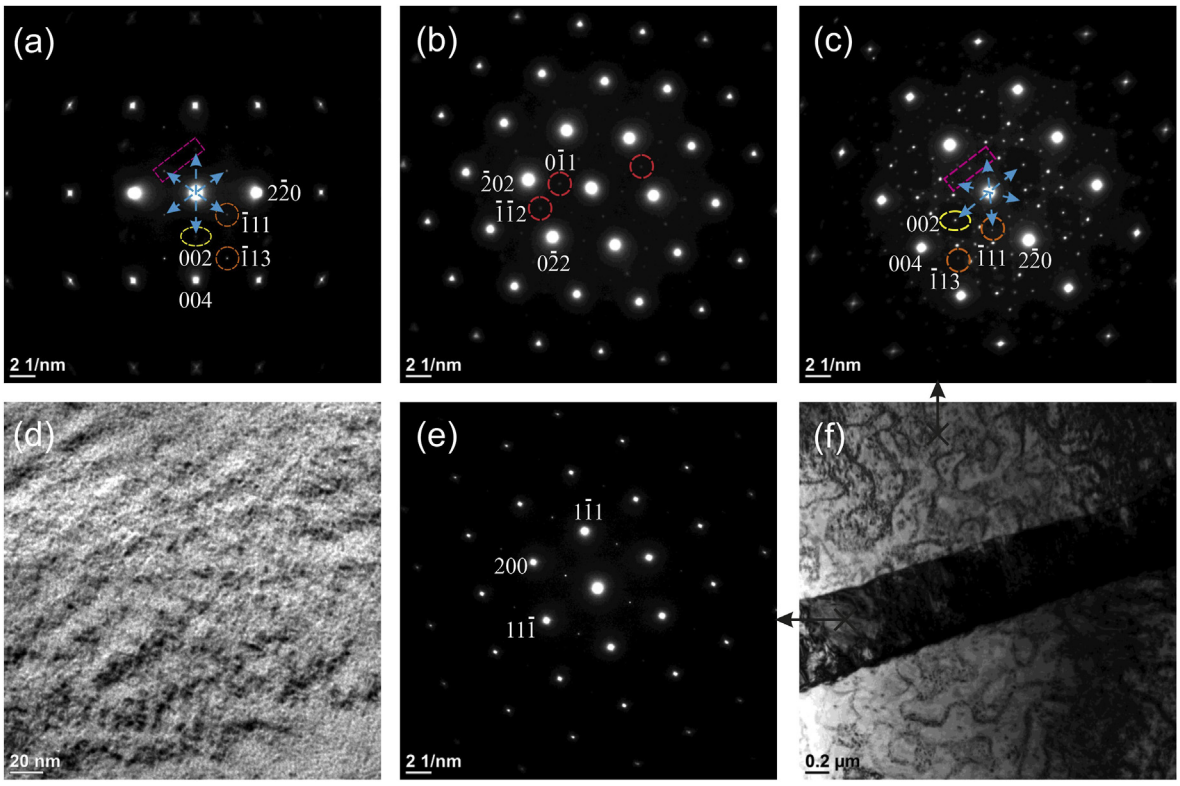

Fig. 5. TEM results for Fe−26.9%Ga; (a and d) for the as cast state and (b, c, e, and f) for samples annealed at 300 °C for 300 h; (a) SADP taken on the A2/$D0_3$ matrix, (d) BF image for the as-cast sample. (f) BF image for the annealed sample showing the precipitation of the $L1_2$ phase along the A2/$D0_3$ grain boundary, (e) SADP for $L1_2$, (b) and (c) SADPs for the A2/$D0_3$ matrix. (a), (c) and (e) SADPs taken with zone axis direction is along [011], (b) SADP taken with zone axis direction along [111] for (c).

the magnetization in the temperature range of 275−425 °C due to the A2 → $D0_3$ and subsequently the $D0_3$ → A2 transition. This effect exists in the Fe−18.6 and 19.5%Ga alloys, too, but at higher temperatures (Fig. 3a). These results confirm unambiguously our recommendation for shifting the first equilibrium boundary to a lower Ga content.

The Fe−25.5%Ga alloy exhibits almost the same behavior as Fe−26.9%Ga, whereas the peak for the one phase $L1_2$ structure does not appear in Fe−24.5%Ga (Fig. 3a and b). This supports the presence of the (A2 + $L1_2$)/$L1_2$ boundary between 24.5 and 25.5% Ga. The smaller height for the $L1_2$ peak shown by Fe−28.9%Ga and the existence of a minor shallow part with a small inclination angle is due to the appearance of a small amount of the Fe_6Ga_5 phase during heating besides $L1_2$.

In the Fe_3Ga type alloy, a nose of the TTT curve is close to 475 °C [17]. The kinetics and morphology of the phase transition from a metastable to the equilibrium ($L1_2$) state for Fe−27.4%Ga are studied by an orientation imaging microscopy using the EBSD analysis. Fig. 4a–f, demonstrate the gradual nucleation and growth of the $L1_2$ phase (red color) at grain boundaries of the $D0_3$ phase (green). The $L1_2$ phase starts to nucleate slowly at the grain boundaries showing moderate growth rates until it covers almost all boundaries after 35 min of annealing (Fig. 4c). By increasing the annealing time, the growth rate for the $L1_2$ phase increases until its fraction reaches 90% at 90 min. For longer annealing times (>90 min), the $L1_2$ phase grows slower to approach 100%. Fig. 4g summarizes the kinetics of this transition. It is notable that the transition rate of the $D0_3$ to $L1_2$ reaction increases in the presence of magnetic field [23].

The details of the two-phase state are clarified by using the results of the TEM study on the Fe−26.9%Ga sample. A small amount of the $L1_2$ phase forms precipitations at the grain boundary between two $D0_3$ grains in the Fe−26.9%Ga sample annealed at 300 °C for 300 h, as shown in Fig. 5. The Fe−26.9%Ga as-cast sample

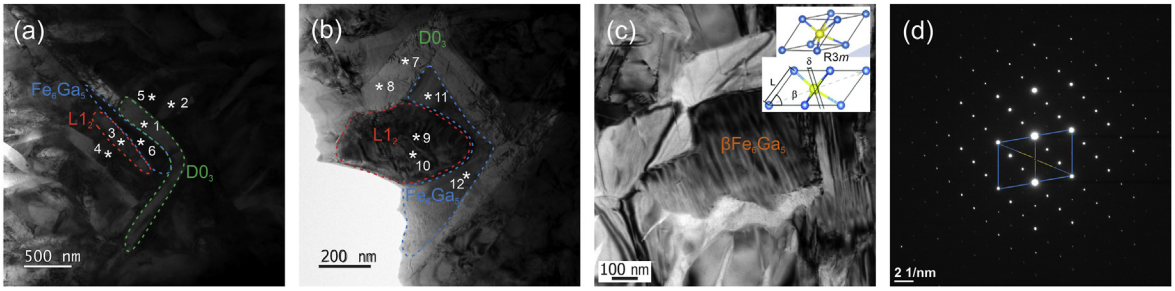

Fig. 6. TEM; BF images for Fe−32.9%Ga annealed at 450 °C for 300 h (a), for the same sample with a higher magnification (b), for Fe−38.4%Ga annealed at 500 °C for 8 h (c), and DP for the latter one (d).

shows a A2/$D0_3$ matrix as revealed by the bright field (BF) image, Fig. 5a. Fig. 5f shows the annealed sample with $L1_2$ precipitates in the A2/$D0_3$ matrix. The selected area diffraction patterns (SADP) taken along the [011] zone axis for the as cast and annealed states are shown in Fig. 5a and c, respectively. The superlattice diffraction spot (002) originates from the *m*-$D0_3$ phase in agreement with [21]. The additional weak spots surrounded by a light red rectangle close to the (002) diffraction spot may be related to surface oxidation according to Refs. [24,25]. The indexed superlattice diffraction spots (113) and (111) correspond to the $D0_3$ phase. The ratio between the intensities of the (002) and (111) reflections is about 2 for both states, while the ratio should be 1 for the single $D0_3$ phase [25]. Thus, the TEM measurements substantiate a phase mixture of $D0_3$ and A2 matrices in the as-cast sample, which confirms the results in Refs. [19,21]. In Fig. 5c, the two reflections indicated by the two arrows also correspond to surface oxidation, and it is obvious that two crossed reflections from two phases are present. The SADP for the annealed sample taken along the [111] zone axis confirms the presence of the tetragonal *m*-$D0_3$ ($L6_0$) phase due to the superlattice diffraction spots observed in Fig. 5b. The BF image for the annealed sample shows that it is composed of mainly the $D0_3$ phase with some fine precipitates with an approximate size of a few tens nanometers on anti-phase boundaries and other plate-like precipitates (see Fig. 5f) in agreement with [25].

The alloys with Ga contents higher than 30% show, in addition to the $D0_3$ and $L1_2$ phases, two polymorphic types of the Fe_6Ga_5 phase: α and β. A detailed study of the structure of Fe−Ga alloys with a Ga content higher than 30% using complementary procedures including neutron diffraction, electron backscattering pattern (SEM-EBSP), TEM, and in situ methods will be reported in the next paper. EDX was applied to analyze the chemical composition of all the precipitates that originate at the grain boundaries of the metastable phase after long term annealing at 450 °C for Fe−32.9Ga alloy (Fig. 6a and b). BF image and diffraction pattern (DP) for 8 h annealed sample at 500 °C of the Fe−38.4%Ga alloy are shown in Fig. 6c and d, respectively.

Table 1 summarizes the chemical compositions of the areas marked on the BF images for Fe−32.9%Ga annealed at 450 °C. It is obvious from the chemical composition that the Fe_6Ga_5 phase, which is identified by points with 42−45% Ga, appears as dark grey precipitates at the grain boundaries (Fig. 6a and b). Thus, the TEM results are consistent with both SEM-EBSD and XRD results presented in Figs. 1 and 4 with respect to the sample structure after long-term (300 h) annealing.

4. Conclusions

1. The XRD and SEM-EBSD results, revealing the presence of an amount of the $L1_2$ phase in Fe−17.5%Ga annealed at 450 and 500 °C for 300 h, substantiate positioning of the equilibrium boundary between the A2 (α Fe) and the A2 + $L1_2$ regions for Ga<17.5%. This is confirmed by the appearance of a specific peak in the VSM curve. The alloys with Ga contents between ~18.5 and 20.6% show the $L1_2$ phase at higher temperatures as compared to the existing Fe−Ga phase diagrams. The location of the phase boundary is completely identified by the XRD results, as shown in Fig. 1.
2. With respect to the position of the phase boundary between the A2+$L1_2$ and $L1_2$ regions, our results match perfectly the equilibrium boundary on the phase diagram proposed by J. Bras [9]. This fact is supported by the appearance of a single $L1_2$ phase after annealing of Fe−25.5 and 26.1%Ga at 450 and 500 °C for 300 h, and the similarity of the corresponding VSM curves to that for the Fe−26.9%Ga alloy.
3. XRD and VSM confirm the position for the equilibrium boundary between $L1_2$ and $L1_2$+α Fe_6Ga_5 recorded by Köster et al. [3], O. Kubaschewski [11] and Okamoto [8].

Table 1
Chemical composition for each point in Fig. 6a and b by EDX.

Phase	Ga, %	Fe, %	No.
$D0_3$	26.9	73.1	1
$L1_2$	26.7	73.3	2
$L1_2$	25.7	74.3	3
Fe_6Ga_5	42.5	57.5	4
Fe_6Ga_5	35.8	64.2	5
Fe_6Ga_5	42.7	57.3	6
$D0_3$	27.7	72.3	7
$D0_3$	26.9	73,1	8
$L1_2$	26.6	73.4	9
$L1_2$	26.5	73.5	10
Fe_6Ga_5	44.2	55.8	11
Fe_6Ga_5	43.8	56.2	12

Author's contributions

AKM performed most experiments, designed, coordinated this research and drafted the manuscript. VVP carried out XRD experiments. VVC examined the samples chemical compositions and performed SEM-EBSD images. ENZ carried out the VSM measurements. WCC performed the TEM test. VK carried out the heat treatment and XRD experiments. SD and GW discussed the results and worked on the manuscript. ISG provided the material studied in this work, discussed about the results, coordinated the research project, and edited the manuscript.

CRediT authorship contribution statement

A.K. Mohamed: Conceptualization, Validation, Formal analysis, Investigation, Writing - original draft, Visualization. **V.V. Palacheva:** Investigation. **V.V. Cheverikin:** Investigation, Writing - original draft, Writing - review & editing. **E.N. Zanaeva:** Investigation. **W.C. Cheng:** Investigation. **V. Kulitckii:** Investigation. **S. Divinski:** Validation, Writing - review & editing. **G. Wilde:** Writing - review & editing. **I.S. Golovin:** Conceptualization, Validation, Writing - review & editing, Supervision, Project administration.

Declaration of competing interest

The authors declare that they have no known competing financial interests or personal relationships that could have appeared to influence the work reported in this paper.

Acknowledgements

The work was carried out with support from RFBR project 18-58-52007. I.S.G. is grateful for DAAD grant Personal ref. no.: 91573930 (2018). W.C.C. would like to thank the Ministry of Science and Technology, Taiwan (Grant no. MOST-107-2923-E-011-003-MY3). We are grateful to Dr. E.M. Bazanova for critical reading of this manuscript and to Mr. Théo Mounier for his help with data proceedings.

Appendix A. Supplementary data

Supplementary data to this article can be found online at https://doi.org/10.1016/j.jallcom.2020.156486.

References

[1] C. Dasarathy, W. Hume-Rothery, The system iron-gallium, Proc. R. Soc. London. Ser. A. Math. Phys. Sci. 286 (1965) 141–157, https://doi.org/10.1098/rspa.1965.0135.

[2] W. Köster, T. Gödecke, Über den Aufbau des Systems Eisen-Gallium zwischen 10 und 50 At.-% Ga und dessen Abhägigkeit von der Wärmebehandlung, I. Das Diagramm der raumzentrierten Phasen, Z. Metallk. 68 (1977) 582–589.

[3] W. Köster, T. Gödecke, Über den Aufbau des Systems Eisen-Gallium z zwischen 10 und 50 At.-% Ga und dessen Abhägigkeit von der Wärmebehandlung II. Das Gleichgewichtsdiagramm, Z. Metallk. 68 (1977) 661–666.

[4] H.L. Luo, Lattice parameters of iron-rich iron-gallium alloys, Trans. Metall. AIME 239 (1967) 119–120.

[5] B. Malaman, M.J. Philippe, B. Roques, A. Courtois, J. Protas, Structures cristallines des phases Fe_6Ge_5 et Fe_6Ga_5, Acta Crystallogr. B 30 (1974) 2081–2087, https://doi.org/10.1107/S0567740874006522.

[6] H.G. Meissner, K. Schubert, Constitution of some systems homologous and quasihomologous to T^5-Ga, II. The systems chromium-gallium, manganese-gallium, and iron-gallium and some notes on the systems vanadium-antimony and vanadium-arsenic, Z. Metallk. 56 (1965) 523–530.

[7] K. Schubert, S. Bhan, W. Burkhart, R. Gohle, H.G. Meissner, M. Poetschke, E. Stolz, Structural data on metallic phases, Naturwissenschaften 47 (1960) 303.

[8] H. Okamoto, Binary Alloy Phase Diagrams, second ed., ASM International: Materials Park, USA, 1993.

[9] J. Bras, J.J. Couderc, M. Fagot, J. Ferre, Transformation ordre-desordre dans la solution solide de fer-gallium, Acta Metall. 25 (1977) 1077–1084, https://doi.org/10.1016/0001-6160(77)90137-7.

[10] E.E. Moore, P.E.A. Turchi, A. Landa, P. Söderlind, B. Oudot, J.L. Belof, S.A. Stout, A. Perron, Development of a CALPHAD thermodynamic database for Pu-U-Fe-Ga alloys, Appl. Sci. 9 (2019) 1–25, https://doi.org/10.3390/app9235040.

[11] O. Kubaschewski, Iron-Binary Phase Diagrams, first ed., Springer- Verlag, Berlin, 1982.

[12] W. Köster, T. Gödecke, Über den Aufbau des Systems Eisen-Gallium z zwischen 10 und 50 At.-% Ga und dessen Abhägigkeit von der Wärmebehandlung III. Ein Unterk, Z. Metallk. 68 (1977) 758–764.

[13] O. Ikeda, R. Kainuma, I. Ohnuma, K. Fukamichi, K. Ishida, Phase equilibria and stability of ordered b.c.c. phases in the Fe-rich portion of the Fe–Ga system, J. Alloys Compd. 347 (2002) 198–205, https://doi.org/10.1016/S0925-8388(02)00791-0.

[14] I.S. Golovin, A.K. Mohamed, V.V. Palacheva, V.V. Cheverikin, A.V. Pozdnyakov, V.V. Korovushkin, A.M. Balagurov, I.A. Bobrikov, N. Fazel, M. Mouas, J.-G. Gasser, F. Gasser, P. Tabary, Q. Lan, A. Kovacs, S. Ostendorp, R. Hubek, S. Divinski, G. Wilde, Comparative study of structure and phase transitions in Fe-(25–27)%Ga alloys, J. Alloys Compd. 811 (2019) 152030, https://doi.org/10.1016/j.jallcom.2019.152030.

[15] I.S. Golovin, A.M. Balagurov, V.V. Palacheva, I.A. Bobrikov, V.B. Zlokazov, In situ neutron diffraction study of bulk phase transitions in Fe-27Ga alloys, Mater. Des. 98 (2016) 113–119, https://doi.org/10.1016/j.matdes.2016.03.016.

[16] V.V. Palacheva, A. Emdadi, F. Emeis, I.A. Bobrikov, A.M. Balagurov, S.V. Divinski, G. Wilde, I.S. Golovin, Phase transitions as a tool for tailoring magnetostriction in intrinsic Fe-Ga composites, Acta Mater. 130 (2017) 229–239, https://doi.org/10.1016/j.actamat.2017.03.049M.V.

[17] I.S. Golovin, A.K. Mohamed, I.A. Bobrikov, A.M. Balagurov, Time-temperature-transformation from metastable to equilibrium structure in Fe-Ga, Mater. Lett. 263 (2020) 127257, https://doi.org/10.1016/j.matlet.2019.127257.

[18] Matyunina, M.A. Zagrebin, V.V. Sokolovskiy, O.O. Pavlukhina, V.D. Buchelnikov, A.M. Balagurov, I.S. Golovin, Phase diagram of magnetostrictive Fe-Ga alloys: insights from theory and experiment, Phase Transit. 92 (2019) 101–116, https://doi.org/10.1080/01411594.2018.1556268.

[19] I.S. Golovin, A.M. Balagurov, I.A. Bobrikov, S.V. Sumnikov, A.K. Mohamed, Cooling rate as a tool of tailoring structure of Fe-(9–33%)Ga alloys, Intermetallics 114 (2019) 106610, https://doi.org/10.1016/j.intermet.2019.106610.

[20] I.S. Golovin, V. Palacheva, A. Mohamed, A.M. Balagurov, I.A. Bobrikov, N. Samoylova, S. Sumnikov, Phase transitions in metastable Fe-Ga alloys, in: SENSORDEVICES 2019, IARIA, Nice, France,, 2019, pp. 13–16.

[21] T. Jin, H. Wang, I.S. Golovin, C. Jiang, Microstructure investigation on magnetostrictive Fe100-xGax and (Fe100-xGax)99.8Tb0.2 alloys for $19 \leq x \leq 29$, Intermetallics 115 (2019) 106628, https://doi.org/10.1016/j.intermet.2019.106628.

[22] J. Gou, T. Yang, X. Liu, T. Ma, Internal structure evolution of $L1_2$ variants in aged Fe-Ga alloys, J. Alloys Compd. 835 (2020) 155282, https://doi.org/10.1016/j.jallcom.2020.155282.

[23] V.A. Milyutin, I.V. Gervasyeva, D.A. Shishkin, YuN. Gornostyrev, E. Beaugnon, I.A. Bobrikov, A.M. Balagurov, A.K. Mohamed, I.S. Golovin, Effect of high magnetic field on the phase transition in Fe-24%Ga and Fe-27%Ga during isothermal annealing, J. Magn. Magn. Mater. (Submitted).

[24] Q. Xing, T.A. Lograsso, Phase identification of quenched Fe-25at.% Ga, Scr. Mater. 60 (2009) 373–376, https://doi.org/10.1016/j.scriptamat.2008.11.007.

[25] Q. Xing, Y. Du, R.J. McQueeney, T.A. Lograsso, Structural investigations of Fe-Ga alloys: phase relations and magnetostrictive behavior, Acta Mater. 56 (2008) 4536–4546, https://doi.org/10.1016/j.actamat.2008.05.011.